

Novel Example-Based Method for Super-Resolution and Denoising of Medical Images

Dinh-Hoan Trinh, *Member, IEEE*, Marie Luong, *Member, IEEE*, Françoise Dibos, Jean-Marie Rocchisani, Canh-Duong Pham, and Truong Q. Nguyen, *Fellow, IEEE*

Abstract—In this paper, we propose a novel example-based method for denoising and super-resolution of medical images. The objective is to estimate a high-resolution image from a single noisy low-resolution image, with the help of a given database of high and low-resolution image patch pairs. Denoising and super-resolution in this paper is performed on each image patch. For each given input low-resolution patch, its high-resolution version is estimated based on finding a nonnegative sparse linear representation of the input patch over the low-resolution patches from the database, where the coefficients of the representation strongly depend on the similarity between the input patch and the sample patches in the database. The problem of finding the nonnegative sparse linear representation is modeled as a nonnegative quadratic programming problem. The proposed method is especially useful for the case of noise-corrupted and low-resolution image. Experimental results show that the proposed method outperforms other state-of-the-art super-resolution methods while effectively removing noise.

Index Terms—Example-based super-resolution, denoising, medical imaging, sparse representation.

I. INTRODUCTION

IMAGES with high resolution are desirable in many applications, such as medical imaging, video surveillance, astronomy, etc. In medical imaging, images are obtained for medical purposes, providing information about the anatomy, the physiologic and metabolic activities of the volume below the skin. The arrival of digital medical imaging technologies

Manuscript received November 16, 2013; accepted January 30, 2014. Date of publication February 25, 2014; date of current version March 18, 2014. The associate editor coordinating the review of this manuscript and approving it for publication was Prof. Marios S. Pattichis.

D.-H. Trinh and C.-D. Pham are with the Center for Informatics and Computing, Vietnam Academy of Science and Technology, Hanoi 10 999, Vietnam (e-mail: tdhoan@cic.vast.vn; pcduong@cic.vast.vn).

M. Luong is with the Laboratoire de Traitement et Transport de l'Information, Université Paris 13, Sorbonne Paris Cité, Villetteuse 93430, France (e-mail: marie.luong@univ-paris13.fr).

F. Dibos is with the Laboratoire Analyse, Géométrie et Applications, Université Paris 13, Sorbonne Paris Cité, Villetteuse 93430, France (e-mail: dibos@math.univ-paris13.fr).

J.-M. Rocchisani is with the University Hospitals Paris-Seine-Saint Denis, Bobigny 93066, France, and also with the Université Paris 13, Sorbonne Paris Cité, Villetteuse 93430, France (e-mail: rocchisani@univ-paris13.fr).

T. Q. Nguyen is with the Department of Electrical and Computer Engineering, University of California, San Diego, CA 92093 USA (e-mail: tqn001@ucsd.edu).

This paper has supplementary downloadable material available at <http://ieeexplore.ieee.org>, provided by the author. The material includes software of a Matlab implementation including a Demo Code for image super-resolution by SRSW method. The total size of the file is 21 MB. Contact marie.luong@univ-paris13.fr for further questions about this work.

Color versions of one or more of the figures in this paper are available online at <http://ieeexplore.ieee.org>.

Digital Object Identifier 10.1109/TIP.2014.2308422

such as Computerized Tomography (CT), Positron Emission Tomography (PET), Magnetic Resonance Imaging (MRI), as well as combined modalities, e.g. SPECT/CT has revolutionized modern medicine [1], [2]. Despite the advances in acquisition technology and the performance of optimized reconstruction algorithms over the two last decades, it is not easy to obtain an image at a desired resolution due to imaging environments, the limitations of physical imaging systems as well as quality-limiting factors such as noise and blur. Noise which is inherent in medical imaging, may reduce adversely the contrast and the visibility of details that could contain vital information, thus compromising the accuracy and the reliability of pathological diagnosis.

Enhancing spatial resolution is an alternative solution to improving resolution, i.e. to detect and discriminate the smallest possible details that can be seen, providing hence a helpful aid for better detection and diagnosis accuracy. This issue has attracted researchers with high interest for medical applications (e.g. [3] for PET images; [4], [5] for MRI; [6] for Ultrasound; [7], [8]). How to enhance spatial resolution while effectively reducing noise is still a challenging problem in medical imaging especially when the images are severely corrupted by noises.

The conventional and well-known interpolation techniques [9]–[11] for enhancing image resolution are unfortunately inefficient when the given low-resolution image is corrupted by noise. Moreover, these techniques may also introduce blurring, ringing, as well as aliasing artifacts. Another technique to alleviate this problem is super-resolution (SR) which consists of generating a high-resolution (HR) image from a low-resolution (LR) image, using additional information such as multiple low-resolution (LR) images or a database that learns relationship between low and high-resolution images. A good overview of the SR methods can be found in [12]–[14]. Since the first idea was introduced by Huang and Tsai [15], many SR methods have been proposed and can be broadly categorized into two main groups: multi-image SR [15]–[18] and single-image SR [19]–[33].

In the multi-image super-resolution method, a HR image is reconstructed by exploiting information from different sub-pixel shifted LR images of the same scene. A typical solution for super-resolution from an image sequence involves three sub-tasks: registration, fusion and deblurring. The first and most important task of these methods is motion estimation or registration between LR images because the precision of the estimation is crucial for the success of the whole method [12].

However, it is difficult to accurately estimate motions between multiple blurred and noisy LR images in applications involving complex movements. This is the reason why multi-image-based SR methods is not ready for practical applications.

The single-image SR methods, also known as example-learning-based methods, have received considerable attention in recent years, since it has emerged as an efficient solution to the spatial resolution enhancement problem. An advantage of these methods is that they do not require many LR images of the same scene as well as registration. In these methods, an image is considered as a set of image patches and SR is performed on each patch. As its name implies, the focus of single-image super resolution is to estimate a high-resolution (HR) image with just a single low-resolution image, and missing high frequency details are recovered based on learning the mapping between low and high-resolution (HR) image patches from a database constructed from examples.

Many learning-based methods have been proposed with demonstrated promising results. Some methods are based on nearest neighbor search, e.g. [23]–[27], [34]. In these methods, each patch of the LR image is compared to the LR patches stored in the database in order to extract the nearest LR patches and hence the corresponding HR patches. These HR patches are then used to estimate the output via different schemes. In [23], Freeman *et al.* used a Markov network to probabilistically model relationships between HR and paired LR patches, and between neighboring HR patches with an approximate solution using belief propagation. In [24], Chang *et al.* proposed to determine the HR patch based on a linear combination of HR patches. For that, after finding the linear combination of the nearest LR neighbors such that it is closest to a given input LR patch, the output HR patch is estimated by replacing LR patches with the associated HR patches in the linear combination. In [28], Kim *et al.* exploited the relationship between HR and LR patch pairs based on a regression function. Despite the success of the nearest neighbor-based methods, the drawback of these methods is that they highly depend on the number of nearest neighbors. More recently, some example-based SR methods via sparse representation have been proposed with promising performances [29]–[31], [35]–[37]. Unlike the nearest neighbor-based methods, these sparse-coding-based SR methods rely on learning the sparse association between image patches, thus avoiding to choose the number of nearest neighbors.

Although many state-of-the-art methods have been proposed, one of the issues of the example-based super-resolution is that it highly depends on the database of low and high-resolution patch pairs. Conventionally, the database is established from extrinsic large dataset. However, some recent works, such as [19], [22], have developed an interesting approach, for which the database can be extracted directly from the LR input, by exploiting the patch redundancy among in-scale and cross-scale images in an image pyramid to enforce constraints for reconstructing the unknown HR image. Another challenge is the questionable performance of these methods when dealing with noisy images. As shown in [30], most of example-learning-based super-resolution algorithms assume that the input images are free of noise. Such assumption is

not likely to be satisfied in real applications such as medical imaging. To deal with noisy data, many existing methods proposed two disjoint steps: first denoising and then super-resolution. The limitation of such strategy is that artifacts can be created during the denoising step and magnified in the subsequent super-resolution step. Moreover, the performance of the method depends on the specific denoising technique. More interestingly, some sparse-coding-based SR methods [30], [38] have achieved promising performance in robustness to image corruptions such as noise, due to the sparse representation [39]. However, these methods can deal with small level of noise. Aiming to solve this problem, we focus on designing a novel example-based SR method for medical images which are often corrupted by noise, by integrating efficiently denoising and super-resolution in the same framework.

As mentioned above, the main limitation of these methods is that their effectiveness highly depends on the supporting database of example images. However, in medical imaging, we observe the interesting fact that many images were acquired at approximately the same location. Thus, we can collect similar (same organ, same modality) and good quality (proven by experts) images and use them as examples to establish a database of low and high resolution image patch pairs. Such example images are referred to as standard images with respect to an input LR image. The proposed method is performed patch-wise with the help of a given set of example images. For an input LR image, a given set of standard images is used to construct a database of example high/low-resolution image patch pairs. This database will be used for the patch SR before the entire HR reconstruction.

After some initial works in [37] and [40], we propose in this paper further development and contributions mainly in the database, the patch SR and extensive experiments on robustness to noise. In the database construction, unlike [37], [40], we construct normalized examples of high/low-resolution image patch pairs. In the HR patch step, it is assumed that each HR patch can be represented as a sparse non-negative linear combination of the example HR patches in the database. To estimate each HR patch from a given LR patch, the idea lies in finding the most consistent example HR patches from the database, to perform the patch SR via a non-negative sparse decomposition model where dissimilarity penalty is integrated. To prevent inconsistent example patches from contaminating the estimation of the HR patch, we introduce a statistical dissimilarity metric as penalty function. However, due to the fact that the desired HR patch is not available, the dissimilarity between the desired HR patch and example HR patches is evaluated through their LR versions. Hence, the example candidates which are not similar with respect to the statistical measure will not be used in the estimation of the HR patch. More precisely, for each given LR patch, we estimate its HR version as a sparse positive linear combination of the HR patches in the database with two conditions: (*i*) the HR estimated version should be consistent with the LR patch under consideration, and (*ii*) the coefficients of the sparse positive linear combination must depend on the similarity between the input LR patch and the example LR patches in the database.

To this end, an optimal model is proposed to find this combination by formulating the SR problem as a constrained optimization one with penalization realized by the proposed criterion of dissimilarity between patches. The proposed SR method has some advantages as follows:

- 1) It can be effectively applied in both cases: the input LR image is a noiseless image or a noisy one. For the noiseless case, the database of example image pairs can be constructed directly using only this LR image.
- 2) Compared with the nearest neighbors-based methods, the proposed sparsity-based method is not limited by the choice of the number of nearest neighbors.
- 3) Unlike the conventional SR methods via sparse representation, the proposed method efficiently exploits the similarity between image patches, and does not train any dictionary.

Experimental results show that the proposed method yields excellent SR results as well as effectively removes noise. It is referred to as SRSW (Super-Resolution by Sparse Weight).

The rest of this paper is organized as follows. Section II presents some related works. Section III describes the proposed method. Our experimental results and comparison with several existing methods are reported in Section IV. The conclusion and future works are presented in Section V.

II. RELATED WORKS

Let us recall the problem of example-learning-based SR. Assume that we are given a set of example images (high quality images) and a LR image \mathbf{Y} generated from the original HR image \mathbf{X} by the model,

$$\mathbf{Y} = D_s H \mathbf{X} + \eta, \quad (1)$$

where H is the blur operator, D_s is the decimation operator with factor s , and η is the additive noise component. The SR reconstruction problem is to estimate the underlying HR version \mathbf{X} of \mathbf{Y} . In the example-based SR methods, an image is considered as an arranged set of image patches and the super-resolution is performed on each patch. Conventionally, an example-based SR method consists of two main phases: *database construction* and *super-resolution*. In the first phase, a set of LR and HR image patch pairs $\{(\mathbf{p}_i^l, \mathbf{p}_i^h), i \in \mathcal{I}\}$ is first extracted from the example images, where \mathcal{I} is the index set. Then, the database, denoted by $(\mathbf{P}_l, \mathbf{P}_h) = \{(\mathbf{u}_i^l, \mathbf{u}_i^h) \in \mathbb{R}^m \times \mathbb{R}^n\}, i \in \mathcal{I}$, of vector pairs is defined as,

$$\mathbf{u}_i^l = \mathbf{F}_l \mathbf{p}_i^l \text{ and } \mathbf{u}_i^h = \mathbf{F}_h \mathbf{p}_i^h \quad (2)$$

where \mathbf{F}_l , \mathbf{F}_h are the operators extracting the features of the LR and HR patches such as edge information, contours, first- and second-order derivatives. In the super-resolution phase, a set of feature vectors of image patches is first extracted from the LR input image \mathbf{Y} , in a similar way as \mathbf{P}_l , and denoted as $\{\mathbf{y}_j^l\} \subset \mathbb{R}^m$. Then, the missing high frequency components $\{\mathbf{x}_j^h\} \subset \mathbb{R}^n$ in the corresponding HR patches of the HR output image \mathbf{X} are estimated based on the co-occurrence relationship between vector pairs $(\mathbf{u}_i^l, \mathbf{u}_i^h)$ in the database $(\mathbf{P}_l, \mathbf{P}_h)$. In this work, for each LR input \mathbf{y}_j^l , \mathbf{x}_j^h is the corresponding HR output.

In this section, we will briefly present the SR method through Neighbor Embedding [24] and the sparse coding-based SR methods [29]–[31], which are both related to our work.

A. Super-Resolution Through Neighbor Embedding

Neighbor-embedding-based (NE) algorithms for super-resolution [24] is performed in two independent processes to synthesize HR image patches. In the first process, for each LR input \mathbf{y}_j^l , K nearest neighbors $\{\mathbf{u}_i^l\}_{i=1}^K$ are searched from the database using the Euclidean distance metric, and thus we have K corresponding HR candidates $\{\mathbf{u}_i^h\}_{i=1}^K$ for the desired HR output \mathbf{x}_j^h . In the second process, \mathbf{x}_j^h is estimated as a weighted combination of the K candidates,

$$\mathbf{x}_j^h = \sum_{i=1}^K \hat{\alpha}_i \mathbf{u}_i^h \quad (3)$$

where the optimal weights $\hat{\alpha}_i$ are determined by solving a constrained least squares problem,

$$\min_{\{\alpha_i\}} \left\| \mathbf{y}_j^l - \sum_{i=1}^K \alpha_i \mathbf{u}_i^l \right\|_2^2 \text{ subject to } \sum_{i=1}^K \alpha_i = 1. \quad (4)$$

In general, the performance of the NE-embedding method is limited by the parameter K and the quality of the K candidates. Fixing K for each low resolution patch may result in overfitting or underfitting. On the other hand, the gradient informations is used to define the feature vectors \mathbf{u}_i^l and \mathbf{y}_j^l which represent geometric structure of the image patches. Unfortunately, this is one of the reasons why the NE method is often less effective when the LR image is corrupted by noise. Indeed, the gradient of a noise-free image and one of its noisy version is very different. Thus, there exists a significant difference between the feature vector \mathbf{u}_i^l in the training database and the feature vector \mathbf{y}_j^l of the noisy patch. Consequently, this affects the quality of K searched nearest neighbors and hence the quality of the output image [an example can be seen in Fig. 8(c)].

B. Sparse-Coding-Based Super-Resolution (ScSR)

The NE method is a promising idea except that it carries out two independent processes to synthesize HR image patches: Searching for K candidates from the database, and estimating the best combination of the K candidates. Hence, a better idea is to address the two phases simultaneously. This idea has been realized very successfully in the sparse-coding-based methods [29]–[31], [35], [36].

The goal of sparse coding is to represent an input vector approximately as a weighted linear combination of a small number of basis vectors called basis atoms. Suppose that the matrix $\mathbf{D} \in \mathbb{R}^{d \times K}$ ($d < K$) is an over-complete dictionary, in which each column vector is a d -dimension atom. Given a vector $\mathbf{y} \in \mathbb{R}^d$, its sparse representation can be determined by finding a sparse solution $\boldsymbol{\alpha} = [\alpha_1, \dots, \alpha_K]^T \in \mathbb{R}^K$ of the following optimization problem:

$$\min_{\boldsymbol{\alpha}} \|\boldsymbol{\alpha}\|_p \text{ subject to } \|\mathbf{y} - \mathbf{D}\boldsymbol{\alpha}\|_2^2 \leq \epsilon, \quad (5)$$

where $\|\boldsymbol{\alpha}\|_p$ is ℓ_p -norm (p is often satisfy $0 \leq p \leq 1$), it is $\|\boldsymbol{\alpha}\|_p = (\sum_i |\alpha_i|^p)^{\frac{1}{p}}$ with $p > 0$, and $\|\boldsymbol{\alpha}\|_0 = \lim_{p \rightarrow 0} \|\boldsymbol{\alpha}\|_p^p$ is the ℓ_0 pseudo-norm which counts the non-zero entries in $\boldsymbol{\alpha}$. Given a training data $\{\mathbf{y}_i, i = 1, \dots, N\}$, the problem of learning a dictionary for sparse-coding is to solve the following optimization problem:

$$\begin{aligned} \min_{\mathbf{D}, \{\boldsymbol{\alpha}^i\}_{i=1}^N} \quad & \sum_{i=1}^N \|\mathbf{y}_i - \mathbf{D}\boldsymbol{\alpha}^i\|_2^2 + \lambda \|\boldsymbol{\alpha}^i\|_p \\ \text{subject to} \quad & \|\mathbf{D}(:, k)\|_2 \leq 1, \forall k = 1, \dots, K, \end{aligned} \quad (6)$$

where λ is a parameter controlling the sparsity penalty and the representation fidelity, and $\mathbf{D}(:, k)$ denotes the k^{th} column of \mathbf{D} .

The SR problem via sparse representation is often performed in two phases: training phase and SR phase.

- *Training phase*: From the database of example vector pairs, $\{(\mathbf{u}_i^l, \mathbf{u}_i^h), i \in \mathcal{I}\}$, a coupled dictionary pair \mathbf{D}_l and \mathbf{D}_h is trained such that the sparse representation of \mathbf{u}_i^l in terms of \mathbf{D}_l is the same as that of \mathbf{u}_i^h in terms of \mathbf{D}_h . Conventionally, \mathbf{D}_l and \mathbf{D}_h are determined by minimizing the following problem [30]:

$$\begin{aligned} \min_{\mathbf{D}_l, \mathbf{D}_h, \{\boldsymbol{\alpha}^i\}_{i=1}^N} \quad & \sum_{i \in \mathcal{I}} (\|\mathbf{u}_i^l - \mathbf{D}_l \boldsymbol{\alpha}^i\|_2^2 + \|\mathbf{u}_i^h - \mathbf{D}_h \boldsymbol{\alpha}^i\|_2^2 + \lambda \|\boldsymbol{\alpha}^i\|_p) \\ \text{subject to} \quad & \|\mathbf{D}_l(:, k)\|_2 \leq 1, \|\mathbf{D}_h(:, k)\|_2 \leq 1, \forall k. \end{aligned} \quad (7)$$

- *SR phase*: To estimate the HR output \mathbf{x}_j^h from the LR input \mathbf{y}_j^l , the sparse representation of \mathbf{y}_j^l in terms of \mathbf{D}_l is first determined by solving the sparse-coding problem:

$$\hat{\boldsymbol{\alpha}}^j = \arg \min_{\boldsymbol{\alpha}^j} \|\mathbf{y}_j^l - \mathbf{D}_l \boldsymbol{\alpha}^j\|_2^2 + \lambda \|\boldsymbol{\alpha}^j\|_p. \quad (8)$$

When $\hat{\boldsymbol{\alpha}}^j$ is obtained, the corresponding HR output can be reconstructed as $\mathbf{x}_j^h = \mathbf{D}_h \hat{\boldsymbol{\alpha}}^j$.

Similar to the NE-embedding methods, the feature vectors \mathbf{y}_j^l and \mathbf{u}_i^l for the LR patches are defined using the first- and second-order derivatives of these LR patches. In [30], it is shown that the ScSR methods can be applied with noisy data. However, logically, this is not an effective way to process with noisy images, due to the possible existence of significant difference between the derivative of a noise-free image and the derivative of its noisy version. The result can be affected adversely, as it can be seen in Fig. 8(d).

As presented above, the K -nearest neighbor-based methods are often limited by the choice of K and the quality of the nearest neighbors. Due to blurring, downsampling, and noisy data, it is very difficult to propose an ideal metric for measuring the similarity between image patches. The sparse coding-based SR methods are proposed to perform SR via sparse representation while avoiding the problem of finding the nearest neighbors. Unlike the K -nearest neighbor-based methods, in the conventional sparse representation model, each patch is coded individually without considering other patches, e.g. the similarity between image patches is not considered. Although these methods offer promising performances, learning the dictionary from the database is often time-consuming. Another difficulty is the debatable performance of these methods when dealing with noisy images.

III. THE PROPOSED METHOD

In this section, we introduce a sparse weight model for single image super-resolution. This model is an integrated framework of super-resolution and denoising, providing us both super-resolved and denoised solutions. This method is very suitable for medical images since these images are often affected not only by limited spatial resolution but also by noise, making the structures or objects of interest indistinguishable. This method can improve the detection by enhancing the spatial resolution while removing noise. The basic idea is to find a non-negative sparse representation of the input \mathbf{y}_i^l over the training database $\mathbf{P}_l = \{\mathbf{u}_k^l, k \in \mathcal{I}\}$, in which the non-zero representation coefficients can be assigned to the example patches \mathbf{u}_k^l which are congruent to \mathbf{y}_i^l . We benefit from the advantages of both the sparse coding-based methods and the K -nearest neighbors-based methods.

Before presenting the proposed method in details, let us begin by recalling the image degradation model. Assume that we are given a LR image \mathbf{Y} , generated from a HR image \mathbf{X} by the model (1). Without loss of generality, the image's values in this work are assumed to be positive. Our aim is to estimate the unknown HR image \mathbf{X} from \mathbf{Y} with the help of a given set of standard images $\{\mathbf{A}_h\}$ which are used as examples. As illustration, a standard MRI image of ankle in Fig. 2(d) is used for the construction of the database and then for super-resolving the LR image of ankle in Fig. 3(a).

Similar to the other example-learning-based SR methods, here, each image can be represented as an arranged set of overlapping patches, and then super-resolution is performed on each patch. The LR image \mathbf{Y} will be represented as a set of N overlapping image patches, that is

$$\mathbf{Y} = \{\mathbf{y}_i^l, i = 1, 2, \dots, N\}, \quad (9)$$

where \mathbf{y}_i^l is a $\sqrt{m} \times \sqrt{m}$ image patch and N is the number of patches generated from the image \mathbf{Y} . Note that N depends on the patch size and the sliding distance between adjacent patches. Similarly, the high-resolution image \mathbf{X} can be also represented as a set of the same number N of paired HR patches $\{\mathbf{x}_i^h, i = 1, 2, \dots, N\}$. The size of \mathbf{x}_i^h is set to be $\sqrt{n} \times \sqrt{n}$ where $\sqrt{n} = s\sqrt{m}$. The LR patch and the HR patches are related by

$$\mathbf{y}_i^l = \mathbf{D}_s \mathbf{H} \mathbf{x}_i^h + \boldsymbol{\eta}_i, \quad (10)$$

where $\boldsymbol{\eta}_i$ is the noise in the i^{th} patch. For the sake of simplicity, we assume that the noise

$$\boldsymbol{\eta}_i \sim \mathcal{N}(0, \sigma_i^2) \quad (11)$$

is Gaussian, white, zero-mean, and i.i.d., with variance σ_i^2 . Thus, we can consider \mathbf{y}_i^l as a LR version of the HR patches \mathbf{x}_i^h . Note that in the case where the standard deviation σ_i is unknown, we can estimate it using techniques in [41] or [42]. In the remaining of this paper, image patches are rearranged as vectors, for example, $\mathbf{x}_i^h \in \mathbb{R}^n$ and $\mathbf{y}_i^l \in \mathbb{R}^m$. Hereafter, an image patch also designates its corresponding vector.

In order to estimate \mathbf{X} , the proposed algorithm is also performed in two phases: *database construction phase* and *super-resolution reconstruction phase*.

- In the first phase, a database of HR and LR patch pairs $(\mathbf{P}_l, \mathbf{P}_h) = \{(\mathbf{u}_k^l, \mathbf{u}_k^h), k \in \mathcal{I}\}$ where \mathcal{I} is the index set, is constructed from a given set of the example images (standard images taken at nearly the same locations as the LR image \mathbf{Y}).
- The super-resolution reconstruction phase consists of the HR patch reconstruction (section III-B) and the reconstruction of the entire HR image (section III-C).

In order to obtain a good database, the selection of these example images should be such that they would contain a variety of intensities as well as shapes and very little noise. Since the standard images and the LR image are often taken from nearby locations and thanks to the repetition of local structures of images, small image patches tend to recur many times inside these images. Thereby, we can assume that for a given LR image patch in \mathbf{Y} , a large number of similar patches can be extracted from the database. This property is very important for the success of the proposed method.

A. Database Construction

In this work, the database of patch pairs is constructed in a simple manner as follows. From the example images, a set $\{\mathbf{p}_k^h, k \in \mathcal{I}\}$ of vectorized image patches of size $\sqrt{n} \times \sqrt{n}$ is first extracted. Then, for each \mathbf{p}_k^h , a corresponding vectorized patch $\mathbf{p}_k^l \in \mathbb{R}^m$ is determined by

$$\mathbf{p}_k^l = D_s H \mathbf{p}_k^h. \quad (12)$$

We consider \mathbf{p}_k^h as a HR patch and \mathbf{p}_k^l as the corresponding LR version. Note that, the LR patch \mathbf{p}_k^l is considered as noise-free one. Consequently, we obtain a database of high-resolution/low-resolution patch pairs

$$(\mathbf{P}_l, \mathbf{P}_h) = \left\{ (\mathbf{u}_k^l, \mathbf{u}_k^h) = \left(\frac{\mathbf{p}_k^l}{\|\mathbf{p}_k^l\|}, \frac{\mathbf{p}_k^h}{\|\mathbf{p}_k^h\|} \right), k \in \mathcal{I} \right\}. \quad (13)$$

We denote below the training set as

$$(\mathbf{P}_l, \mathbf{P}_h) = \left\{ (\mathbf{u}_k^l, \mathbf{u}_k^h) \in \mathbb{R}^m \times \mathbb{R}^n, k \in \mathcal{I} \right\}, \quad (14)$$

in which $\|\mathbf{u}_k^l\|_2 = 1$ and $D_s H \mathbf{u}_k^h = \mathbf{u}_k^l$ for all $k \in \mathcal{I}$. We can consider the set \mathbf{P}_l and \mathbf{P}_h as the matrices in $\mathbb{R}^{m \times \text{card}(\mathcal{I})}$ and $\mathbb{R}^{n \times \text{card}(\mathcal{I})}$, respectively. Note that using this construction, we can write $\mathbf{P}_l = D_s H \mathbf{P}_h$.

In the next subsections, we will present in details the proposed super-resolution model. This model consists of two main steps as follows:

- **Step 1. Patch super-resolution** (section III-B): In this step, the sparse weight optimization model is proposed for super-resolution and denoising on image patch. The optimization problem is established such that its solution determines a non-negative sparse linear representation of the input LR patch over the example patches in the database, and a measure of similarity between patches is proposed and used as penalization function to enforce sparsity.
- **Step 2. Reconstruction of the entire HR image** (section III-C): This step allows to aggregate the final HR image using the estimated HR patches in the first step.

B. Sparse Weight Model for Patch Super-Resolution

1) *Formulation*: In this subsection, we will present in details the proposed model for denoising and super-resolution.

Let us consider a LR patch $\mathbf{y}_i^l = D_s H \mathbf{x}_i^h + \boldsymbol{\eta}_i$ as in (10), with the noise component $\boldsymbol{\eta}_i \sim \mathcal{N}(0, \sigma_i^2)$. The problem is to find an estimate of the HR patch \mathbf{x}_i^h , denoted by $\hat{\mathbf{x}}_i^h$, from \mathbf{y}_i^l with the help of the database $(\mathbf{P}_l, \mathbf{P}_h)$. Thanks to the repetition of local structures of images, we can expect that there exists a subset of patches $\mathbf{u}_k^h \in \mathbf{P}_h$ which have similar structures as those in \mathbf{x}_i^h . Such patches will play an important role in determining the estimate $\hat{\mathbf{x}}_i^h$.

In this work, it is assumed that $\mathbf{x}_i^h \in \mathbb{R}^n$ can be represented as a sparse non-negative linear combination of the HR patches in \mathbf{P}_h ,

$$\mathbf{x}_i^h = \sum_{k \in \mathcal{I}} \alpha_{ik} \mathbf{u}_k^h, \quad (15)$$

where the vector of representation coefficients $\boldsymbol{\alpha}^i = [\alpha_{i1}, \alpha_{i2}, \dots, \alpha_{ik}, \dots]^T \geq 0$. Note that unlike the previous ScSR methods in [29], [30], [35], [36], and [31], in (15) we use non-negative constraint on the coefficients α_{ik} . This can be explained by considering both sides of equation (15). Due to the fact that the vectors \mathbf{x}_i^h and \mathbf{u}_k^h are defined from the pixel values of image patches, they are then positive vectors. Thus, in the equation $\mathbf{x}_i^h = \mathbf{P}_h \boldsymbol{\alpha}^i$, both \mathbf{x}_i^h and \mathbf{P}_h are non-negative. This is why we can require the non-negative constraint on $\boldsymbol{\alpha}^i$.

Now, consider the corresponding LR patch \mathbf{y}_i^l of \mathbf{x}_i^h . Since it is assumed that $\mathbf{x}_i^h = \mathbf{P}_h \boldsymbol{\alpha}^i$, multiplying this equation by $D_s H$ gives

$$D_s H \mathbf{x}_i^h = D_s H \mathbf{P}_h \boldsymbol{\alpha}^i = \mathbf{P}_l \boldsymbol{\alpha}^i. \quad (16)$$

By exploiting the relation between the LR and the HR patches, $\mathbf{y}_i^l = D_s H \mathbf{x}_i^h + \boldsymbol{\eta}_i$, we obtain

$$\mathbf{P}_l \boldsymbol{\alpha}^i = \mathbf{y}_i^l - \boldsymbol{\eta}_i. \quad (17)$$

This implies that

$$\mathbf{y}_i^l - \mathbf{P}_l \boldsymbol{\alpha}^i = \boldsymbol{\eta}_i. \quad (18)$$

Thus,

$$\|\mathbf{y}_i^l - \mathbf{P}_l \boldsymbol{\alpha}^i\|_2 \leq \xi_i, \quad (19)$$

where ξ_i is related to the noise power σ_i of $\boldsymbol{\eta}_i$.

As it can be seen, the LR patch \mathbf{y}_i^l can be represented by the same sparse vector $\boldsymbol{\alpha}^i$ over the database of LR patches \mathbf{P}_l , with a controlled error ξ_i . This implies that for a given LR patch \mathbf{y}_i^l , the estimate of the corresponding HR patch \mathbf{x}_i^h is performed by first determining sparse representation vector $\boldsymbol{\alpha}^i$ of \mathbf{y}_i^l with respect to the database of LR patches \mathbf{P}_l . Then, \mathbf{x}_i^h can be recovered by simply multiplying this representation by the database \mathbf{P}_h , $\hat{\mathbf{x}}_i^h = \mathbf{P}_h \boldsymbol{\alpha}^i$. This is the core idea behind the proposed method.

More precisely, our aim is to find the patches \mathbf{u}_k^h which should be similar to \mathbf{x}_i^h and then to use them for the estimation of \mathbf{x}_i^h . Therefore, in order to select the similar patches (in the database) with \mathbf{x}_i^h , we try to force coefficient vector $\boldsymbol{\alpha}^i = [\alpha_{i1}, \alpha_{i2}, \dots, \alpha_{ik}, \dots]^T$ such that most of its zero components, α_{ik} , correspond to the elements \mathbf{u}_k^h which are dissimilar to \mathbf{x}_i^h .

To this end, we formulate the problem of finding the vector α^i as the following sparse decomposition problem:

$$\begin{aligned} \alpha^i &= \arg \min_{\alpha \geq 0} \|\alpha\|_0 + \sum_{k \in \mathcal{I}} w_{ik} \alpha_{ik} \\ \text{subject to } &\|\mathbf{y}_i^l - \sum_{k \in \mathcal{I}} \alpha_{ik} \mathbf{u}_k^l\|_2^2 \leq \epsilon \sigma_i^2, \end{aligned} \quad (20)$$

where $\alpha = [\alpha_{i1}, \alpha_{i2}, \dots, \alpha_{ik}, \dots]^T$, ϵ is a given positive number, σ_i is the standard deviation of the noise in the i^{th} patch, the ℓ_0 -norm assures that the solution α^i is a sparse one, while the positive penalty coefficients w_{ik} depend on the dissimilarity (or inversely the similarity) between \mathbf{x}_i^h and \mathbf{u}_k^h .

By penalizing on α_{ik} , we force small α_{ik} for high dissimilarity w_{ik} , i.e. for weak similarity between \mathbf{x}_i^h and \mathbf{u}_k^h . However, due to the fact that the HR patch \mathbf{x}_i^h is not available, the dissimilarity between \mathbf{x}_i^h and \mathbf{u}_k^h is evaluated using their LR versions \mathbf{y}_i^l and \mathbf{u}_k^l . Thus, in the cases where \mathbf{u}_k^l and \mathbf{y}_i^l are very dissimilar, w_{ik} is large. Then, if α_{ik} is large the term $w_{ik} \alpha_{ik}$ will be penalized with a large cost. In the other hand, with α_{ik} very small or null, the objective function in (20) can be minimized. The constraint term in (20) implies that the output HR patch $\hat{\mathbf{x}}_i^h = \sum_{k \in \mathcal{I}} \alpha_{ik} \mathbf{u}_k^h$ has to be consistent with the input \mathbf{y}_i^l . Therefore, $\hat{\mathbf{x}}_i^h$ can be determined optimally from several example HR patches $\mathbf{u}_k^h \in \mathbf{P}_h$ which have similar structures with the desired patch \mathbf{x}_i^h . Consequently, it can avoid the influence of the inconsistent patches in the determination of the estimate $\hat{\mathbf{x}}_i^h$.

In this work, the penalty coefficients w_{ik} is defined as

$$w_{ik} = \Phi_i(d(\mathbf{y}_i^l, \mathbf{u}_k^l)), \quad (21)$$

where $d : \mathbb{R}^m \times \mathbb{R}^m \rightarrow \mathbb{R}^+$ is a criterion evaluating the dissimilarity between \mathbf{y}_i^l and \mathbf{u}_k^l , while $\Phi : \mathbb{R} \rightarrow \mathbb{R}^+$ is a non-negative increasing function. The value of the function $d(\mathbf{y}_i^l, \mathbf{u}_k^l)$ expresses the dissimilarity between \mathbf{y}_i^l and \mathbf{u}_k^l . A small dissimilarity value $d(\mathbf{y}_i^l, \mathbf{u}_k^l)$ implies a high similarity between \mathbf{y}_i^l and \mathbf{u}_k^l . Normally, to measure the extent of dissimilarity among the image patches, one of the most popular dissimilarity criteria is the Euclidian distance. However, in this case \mathbf{y}_i^l is a vector defined from the pixel values of the i^{th} patch of the input LR image \mathbf{Y} while \mathbf{u}_k^l is a normalized example vector in the database. Moreover, \mathbf{y}_i^l is also corrupted by noise η_i . Thus, using the Euclidian distance may not be effective enough. To obtain a better dissimilarity criterion, let us consider the relationship of \mathbf{y}_i^l and \mathbf{u}_k^l .

We start with definition of congruence of image patches. Two image patches \mathbf{x}_1 and \mathbf{x}_2 are congruent if there exists a non-zero constant $\mu \in \mathbb{R}$, with $\mathbf{x}_1 = \mu \mathbf{x}_2$. As mentioned above, \mathbf{y}_i^l is assumed to be corrupted by Gaussian white noise $\eta_i \sim \mathcal{N}(0, \sigma_i^2)$, with $\mathbf{y}_i^l = D_s H \mathbf{x}_i^h + \eta_i$ (see (10)). Thus, the patch \mathbf{u}_k^l is ideally similar to \mathbf{y}_i^l if \mathbf{u}_k^l is congruent to $D_s H \mathbf{x}_i^h$. That means there exists a constant $\mu_{ik} > 0$ such that

$$\mathbf{y}_i^l = \mu_{ik} \mathbf{u}_k^l + \eta_i. \quad (22)$$

According to the assumption for the noise component $\eta_i \sim \mathcal{N}(0, \sigma_i^2)$, the mean of η_i , $E(\eta_i) \approx 0$. Therefore, the

constant μ_{ik} can be approximately computed as:

$$E(\mathbf{y}_i^l) = \mu_{ik} E(\mathbf{u}_k^l) + \underbrace{E(\eta_i)}_{\approx 0} \implies \mu_{ik} = \frac{E(\mathbf{y}_i^l)}{E(\mathbf{u}_k^l)}. \quad (23)$$

From equation (22), we have $(\mathbf{y}_i^l - \mu_{ik} \mathbf{u}_k^l) \sim \mathcal{N}(0, \sigma_i^2)$. It can be inferred that,

$$\begin{aligned} \frac{E(\mathbf{y}_i^l - \mu_{ik} \mathbf{u}_k^l)}{\text{Var}(\mathbf{y}_i^l - \mu_{ik} \mathbf{u}_k^l) - \sigma_i^2} &\simeq 0 \\ \frac{\text{Var}(\mathbf{y}_i^l - \mu_{ik} \mathbf{u}_k^l)}{\sigma_i^2} &\simeq 0. \end{aligned} \quad (24)$$

Therefore, we propose to use the parameter a_{ik} such that

$$a_{ik} = |E(\mathbf{y}_i^l - \mu_{ik} \mathbf{u}_k^l)| + |\text{Var}(\mathbf{y}_i^l - \mu_{ik} \mathbf{u}_k^l) - \sigma_i^2| \simeq 0. \quad (25)$$

The parameter a_{ik} allows us to evaluate the statistical property of noise in the residual patch. So, in this work, the dissimilarity criterion d is defined by

$$d(\mathbf{y}_i^l, \mathbf{u}_k^l) = \|\mathbf{y}_i^l - \mu_{ik} \mathbf{u}_k^l\|_2^2 + a_{ik}, \quad (26)$$

where μ_{ik} is defined by (23).

In this work, $\Phi_i(\cdot)$ in (21) is defined by $\Phi_i(t) = t$ if $\sigma_i = 0$. Otherwise, if $\sigma_i > 0$ then

$$\Phi_i(t) = \begin{cases} e^t & \text{if } t > \rho_i \\ t & \text{if } t \leq \rho_i \end{cases} \quad (27)$$

where ρ_i is a positive threshold depending on \mathbf{y}_i^l . As can be seen, the function $\Phi_i(t)$ strongly increases when $t > \rho_i$. In other words, the penalty coefficients corresponding to the example patches such that $d(\mathbf{y}_i^l, \mathbf{u}_k^l) > \rho_i$ will be very high. Note that in the ideal case, $\mu_{ik} \mathbf{u}_k^l = D_s H \mathbf{x}_i^h$, we have,

$$d(\mathbf{y}_i^l, \mathbf{u}_k^l) \approx \|\eta_i\|^2 \approx \gamma(m\sigma_i^2), \quad (28)$$

where m is the number of elements in vector \mathbf{y}_i^l ($\mathbf{y}_i^l \in \mathbb{R}^m$), and γ is a positive constant. Therefore, for $d(\mathbf{y}_i^l, \mathbf{u}_k^l) \leq \gamma(m\sigma_i^2)$ we can assume that \mathbf{u}_k^l is congruent with $D_s H \mathbf{x}_i^h$, and thus \mathbf{u}_k^l is congruent with the desired HR patch \mathbf{x}_i^h . Then, the threshold ρ_i in (27) is set to $\gamma(m\sigma_i^2)$.

It is easy to see that the objective in (20) is not a convex function, since ℓ_0 -norm is not a true norm. This problem is too complex to solve in general. To avoid the above problem we replace ℓ_0 -norm by ℓ_1 -norm, and problem (20) becomes convex and can be rewritten as:

$$\begin{aligned} \alpha^i &= \arg \min_{\alpha \geq 0} \|\alpha\|_1 + \sum_{k \in \mathcal{I}} w_{ik} \alpha_{ik} \\ \text{subject to } &\|\mathbf{y}_i^l - \sum_{k \in \mathcal{I}} \alpha_{ik} \mathbf{u}_k^l\|_2^2 \leq \epsilon \sigma_i^2 \end{aligned} \quad (29)$$

$$\Leftrightarrow \alpha^i = \arg \min_{\alpha \geq 0} \sum_{k \in \mathcal{I}} (1 + w_{ik}) \alpha_{ik} \quad (30)$$

$$\text{subject to } \|\mathbf{y}_i^l - \sum_{k \in \mathcal{I}} \alpha_{ik} \mathbf{u}_k^l\|_2^2 \leq \epsilon \sigma_i^2.$$

Lagrange multipliers allow an equivalent formulation

$$\alpha^i = \arg \min_{\alpha \geq 0} \frac{1}{2} \|\mathbf{y}_i^l - \sum_{k \in \mathcal{I}} \alpha_{ik} \mathbf{u}_k^l\|_2^2 + \lambda \sum_{k \in \mathcal{I}} (1 + w_{ik}) \alpha_{ik}, \quad (31)$$

where the parameter λ balances sparsity of the solution and fidelity of the approximation to \mathbf{y}_i^l .

Algorithm 1 Multiplicative Updates Algorithm for NQP [44]

Input: $\alpha = \alpha_0 > 0$, number of iterations T .

Updating: $t = 0$

While $t < T$ & $\|\mathbf{y}_i^l - \mathbf{U}_i \alpha_t\|_2^2 > m\sigma_i^2$

$$\alpha_{t+1} = \alpha_t \cdot^* (\mathbf{U}_i^T \mathbf{y}_i^l) ./ (\mathbf{U}_i^T \mathbf{U}_i \alpha_t + \mathbf{w}_i); \quad (36)$$

$t = t + 1$;

End

Output: $\alpha^i = \alpha_t$.

We can reduce the computation time by imposing a threshold on the dissimilarity criterion d . Let us denote $S(\mathbf{y}_i^l) = \{k \in \mathcal{I} : \alpha_{ik} > 0\}$ as the support set of \mathbf{y}_i^l . As analyzed above, $S(\mathbf{y}_i^l)$ involves \mathbf{u}_k^l where $d(\mathbf{y}_i^l, \mathbf{u}_k^l)$ is not very large. Thus, with a suitable value of the threshold r_i , there exists a subset \mathcal{I}_i of \mathcal{I} ,

$$\mathcal{I}_i = \{j \in \mathcal{I} : d(\mathbf{y}_i^l, \mathbf{u}_j^l) \leq r_i\}, \quad (32)$$

such that

$$S(\mathbf{y}_i^l) \subseteq \mathcal{I}_i. \quad (33)$$

Thus, to save computing time, problem (31) should be considered on the subset \mathcal{I}_i ,

$$\alpha^i = \arg \min_{\alpha \geq 0} \frac{1}{2} \|\mathbf{y}_i^l - \sum_{k \in \mathcal{I}_i} \alpha_{ik} \mathbf{u}_k^l\|_2^2 + \lambda \sum_{k \in \mathcal{I}_i} (1 + w_{ik}) \alpha_{ik}. \quad (34)$$

It is easily to see that problem (34) can be rewritten as:

$$\alpha^i = \arg \min_{\alpha \geq 0} \frac{1}{2} \|\mathbf{y}_i^l - \mathbf{U}_i \alpha\|_2^2 + \mathbf{w}_i^T \alpha \quad (35)$$

where \mathbf{U}_i is the matrix whose columns are the vectors \mathbf{u}_k^l , \mathbf{w}_i is the vector formed by concatenating all the coefficients $\lambda(1 + w_{ik})$, here $k \in \mathcal{I}_i$.

2) *Algorithm:* As it can be seen, (35) is a Non-negative Quadratic Programming (NPQ) which can be effectively solved by many algorithms (see [43]). To solve this problem, we use in this work the multiplicative updates algorithm proposed by Hoyer in [44] (see [44] for details on derivation and convergence).

In (36), the operators \cdot^* and $./$ represent element-wise multiplication and division, respectively.

When α^i is obtained, the desired HR patch $\hat{\mathbf{x}}_i^h$ can be estimated as

$$\hat{\mathbf{x}}_i^h = \sum_{k \in \mathcal{I}_i} \alpha_{ik} \mathbf{u}_k^h. \quad (37)$$

Likely, by considering that the denoised patch $\hat{\mathbf{y}}_i^l$ of \mathbf{y}_i^l is represented as a non-negative sparse linear combination of the LR patch in the database, we can obtain a denoised version $\hat{\mathbf{y}}_i^l$ as follows:

$$\hat{\mathbf{y}}_i^l = \mathbf{U}_i \alpha^i = \sum_{k \in \mathcal{I}_i} \alpha_{ik} \mathbf{u}_k^l. \quad (38)$$

In the next subsection (subsection III-C), we will present how to construct the entire HR image using the estimated HR patches $\hat{\mathbf{x}}_i^h$, and the denoised patches $\hat{\mathbf{y}}_i^l$.

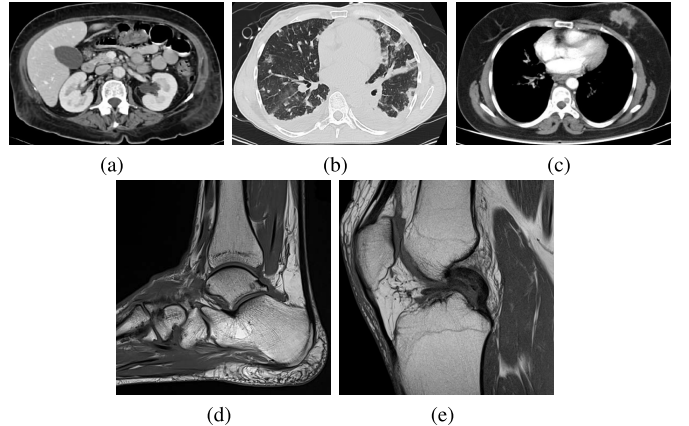


Fig. 1. Test HR images (a) CT image of abdomen of size 540×360 , (b) CT image of thorax of size 540×360 , (c) CT image of chest of size 540×360 , (d) MRI image of ankle of size 400×400 , (e) MRI image of knee of size 400×400 .

C. Reconstruction of the Entire HR Image

To obtain the entire HR image, we first set all the estimated HR patches $\hat{\mathbf{x}}_i^h$ in the proper locations in the HR grid. A coarse estimate of \mathbf{X} , $\hat{\mathbf{X}}^{coarse}$, is then computed by averaging in overlapping regions. In the same way, we obtain a denoised image, denoted by $\mathbf{Y}^{denoise}$, of \mathbf{Y} by replacing the noisy patches \mathbf{y}_i^l by the denoised $\hat{\mathbf{y}}_i^l$, and then performing averaging in overlapping regions.

Similarly to [29], we determine the final HR image $\hat{\mathbf{X}}^{final}$ as the minimizer of the following problem:

$$\min_{\mathbf{X}} \|\mathbf{X} - \hat{\mathbf{X}}^{coarse}\|_2^2 \text{ subject to } D_s H \mathbf{X} = \mathbf{Y}^{denoise}. \quad (39)$$

The iterative back-projection (IBP) algorithm [17] is used to solve this problem:

$$\mathbf{X}_{t+1} = \mathbf{X}_t + ((\mathbf{Y}^{denoise} - D_s H \mathbf{X}_t) \uparrow_s) * p, \quad (40)$$

where \mathbf{X}_t is the estimate of the HR image at the t -th iteration, \uparrow_s denotes up-scaling by factor s , p is a symmetric Gaussian filter. As shown in [45], the convergence condition for the IBP procedure (40) is that $\|\delta - D_s(p * H)\|_1 < 1$, where δ denotes the unity pulse function centered at $(0, 0)$. As mentioned in [17], there is some freedom in the choice of p as long as the convergence condition is satisfied. Here, we use the symmetric Gaussian filter of size 5 with standard deviation 1. Note that in the case where the input LR image \mathbf{Y} can be considered as a noise-free image, $\mathbf{Y}^{denoise}$ in (39) and (40) is replaced by \mathbf{Y} . The entire super-resolution process is summarized as Algorithm 2.

IV. PERFORMANCE EVALUATION

In this section, we present several SR experiments performed on both images with and without noise for magnification factor $s = 4$ to evaluate the effectiveness of the proposed SR method. The proposed method (called SRSW) is compared with the bicubic interpolation (Bb), the Neighbor Embedding-based SR method (NE)¹ of Chang *et al.* [24], and the Sparse coding-based SR method (ScSR)² of Yang *et al.* [30] in terms of both objective and subjective measures.

¹Matlab code: <http://www.jdl.ac.cn/user/hchang/publication.htm>

²Matlab code: <http://www.ifp.illinois.edu/~jyang29/index.html>

Algorithm 2 The Proposed Super-Resolution Algorithm**INPUT:**

- The LR image \mathbf{Y} and the size of LR patch $\sqrt{m} \times \sqrt{m}$.
- Magnification factor s .
- Database $(\mathbf{P}_l, \mathbf{P}_h) = \{(\mathbf{u}_k^l, \mathbf{u}_k^h), k \in \mathcal{I}\}$. $\mathbf{P}_l \in \mathbb{R}^{m \times M}$ and $\mathbf{P}_h \in \mathbb{R}^{n \times M}$.
- Regularization parameter λ in (34), number T of iterations in Algorithm 1.

OUTPUT: HR image $\hat{\mathbf{X}}^{final}$ **BEGIN**

- Partition \mathbf{Y} into an arranged set of N overlapping $\sqrt{m} \times \sqrt{m}$ patches $\{\mathbf{y}_i^l\}_{i=1}^N$.
- For** each patch \mathbf{y}_i^l of \mathbf{Y}
 - Compute the dissimilarity criteria $d(\mathbf{y}_i^l, \mathbf{u}_k^l)$ using (23),(25) and (26).
 - Determine the subset \mathcal{I}_i .
 - If $\sigma > 0$, compute the penalty coefficients \mathbf{w}_i using (21) and (27).
 - Solve the problem (35) using Algorithm 1.
 - Generate the HR patch $\hat{\mathbf{x}}_i^h = \sum_{k \in \mathcal{I}_i} \alpha_{ik} \mathbf{u}_k^h$ and the denoised LR patch $\hat{\mathbf{y}}_i^l = \mathbf{U}_i \boldsymbol{\alpha}_i^l$.
- End**
- Fusion:** Produce the initial HR image $\hat{\mathbf{X}}^{coarse}$ and the denoised image $\mathbf{Y}^{denoise}$.
- IBP enhancement:** Using the IBP procedure (40) on the coarse HR image $\hat{\mathbf{X}}^{coarse}$ to reconstruct the final HR image $\hat{\mathbf{X}}^{final}$.

END**A. Experimental Configuration**

The experimental tests are performed on five 8-bit images used as test HR images and shown in Fig. 1: CT of abdomen, CT of thorax, CT of chest, MRI of ankle, and MRI of knee. The training databases of all the methods are established with the same set of five standard images as illustrated in Fig. 2. For each test image in Fig. 1, a corresponding standard image in Fig. 2 is used as example. In all experiments, the LR image is created from the corresponding test image in three steps: first, the test image is blurred by a 7×7 Gaussian filter with standard deviation 1, then downsampling by a decimation factor of s is performed, and finally the Gaussian white noise with standard deviation σ is added into the decimated image. The experiments are conducted in both noise-free image ($\sigma = 0$) and noisy image ($\sigma = 5, 10$ and 20). For all the methods, super-resolution is realized two times with magnification factor 2.

For the proposed SRSW method, the database includes 150000 patch pairs extracted randomly from the standard images. Default size of the HR patches and LR patches are 9×9 and 5×5 , respectively. The parameter λ in (34) is experimentally set to 0.001, r_i in (32) is chosen such that \mathcal{I}_i is the set of 100 first elements having the smallest values $d(\mathbf{y}_i^l, \mathbf{u}_k^l)$ (the criterion d is defined by (26)). In the case of noise, the threshold ρ_i in (27) is set to $44(m\sigma^2)$. For NE-based

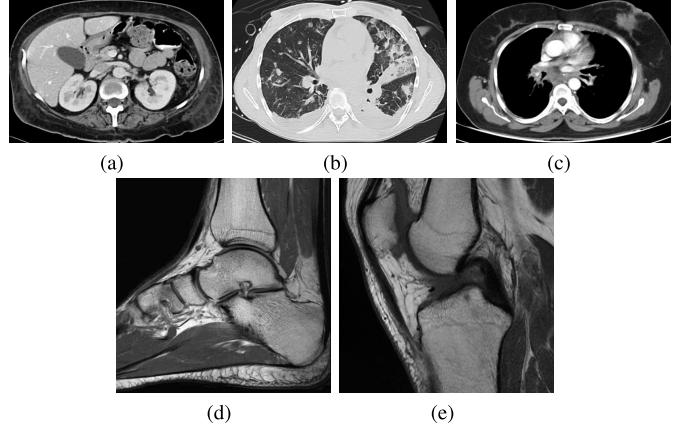


Fig. 2. Standard images used to construct the database (a) CT image of abdomen, (b) CT image of thorax, (c) CT image of chest, (d) MRI image of ankle, and (e) MRI image of knee.

TABLE I
PSNR AND SSIM COMPARISON FOR $4 \times$ MAGNIFICATION

| Image | σ | PSNR (dB) | | | | SSIM | | | |
|-------|----------|-----------|-------|-------|--------------|------|------|-------------|-------------|
| | | Bb | NE | ScSR | SRSW | Bb | NE | ScSR | SRSW |
| (a) | 0 | 26.38 | 27.45 | 28.19 | 28.71 | 0.84 | 0.84 | 0.88 | 0.88 |
| | 5 | 25.96 | 25.94 | 26.54 | 28.71 | 0.77 | 0.78 | 0.80 | 0.88 |
| | 10 | 24.85 | 25.32 | 25.22 | 28.53 | 0.67 | 0.73 | 0.76 | 0.87 |
| | 20 | 22.22 | 23.50 | 23.39 | 24.74 | 0.50 | 0.61 | 0.64 | 0.71 |
| (b) | 0 | 23.71 | 24.31 | 24.93 | 25.04 | 0.71 | 0.72 | 0.76 | 0.76 |
| | 5 | 23.45 | 23.68 | 24.30 | 24.92 | 0.67 | 0.68 | 0.70 | 0.76 |
| | 10 | 22.78 | 23.08 | 23.42 | 24.70 | 0.58 | 0.62 | 0.66 | 0.74 |
| | 20 | 20.82 | 22.20 | 22.08 | 24.45 | 0.42 | 0.53 | 0.58 | 0.72 |
| (c) | 0 | 25.24 | 26.48 | 26.75 | 27.38 | 0.85 | 0.86 | 0.85 | 0.87 |
| | 5 | 24.96 | 24.91 | 25.97 | 27.11 | 0.75 | 0.77 | 0.78 | 0.86 |
| | 10 | 24.19 | 24.29 | 24.86 | 26.99 | 0.64 | 0.71 | 0.76 | 0.85 |
| | 20 | 21.97 | 23.73 | 23.42 | 24.44 | 0.48 | 0.60 | 0.65 | 0.71 |
| (d) | 0 | 24.63 | 24.88 | 25.31 | 25.41 | 0.71 | 0.72 | 0.75 | 0.76 |
| | 5 | 24.36 | 23.69 | 24.79 | 25.41 | 0.65 | 0.61 | 0.66 | 0.75 |
| | 10 | 23.63 | 23.34 | 23.87 | 25.40 | 0.56 | 0.58 | 0.62 | 0.75 |
| | 20 | 21.56 | 22.22 | 22.42 | 25.11 | 0.42 | 0.48 | 0.53 | 0.72 |
| (e) | 0 | 26.46 | 26.73 | 27.11 | 27.25 | 0.69 | 0.70 | 0.72 | 0.73 |
| | 5 | 26.01 | 25.36 | 26.38 | 27.24 | 0.64 | 0.62 | 0.64 | 0.72 |
| | 10 | 24.92 | 24.77 | 25.42 | 27.20 | 0.56 | 0.57 | 0.61 | 0.72 |
| | 20 | 22.16 | 23.16 | 23.56 | 26.73 | 0.42 | 0.48 | 0.52 | 0.68 |

method, to get good results, the number of neighbors reduces as noise increases. For the SC-based method, the robustness to noise is related to the regularization parameter λ [30]. Concretely, the larger the value λ , the higher the capability of the model to suppress noise.

B. Experimental Results

In order to evaluate the objective quality of the super-resolved images, we use two quality metrics, namely *Peak Signal to Noise Ratio* (PSNR) and *Structural SIMilarity* (SSIM) [46]. The PSNR measures the intensity difference between two images. However, it is well-known that it can fail to describe the subjective quality of the image. SSIM is one of the most frequently used metrics for image quality assessment. Compared with PSNR, SSIM better expresses the structure similarity between the recovered image and the reference one. The best results of the methods are reported in Table I and the best value obtained for each noise level is in bold number. We can observe that, for $\sigma = 0$, the quantitative evaluations of the proposed SRSW method are superior to those of the

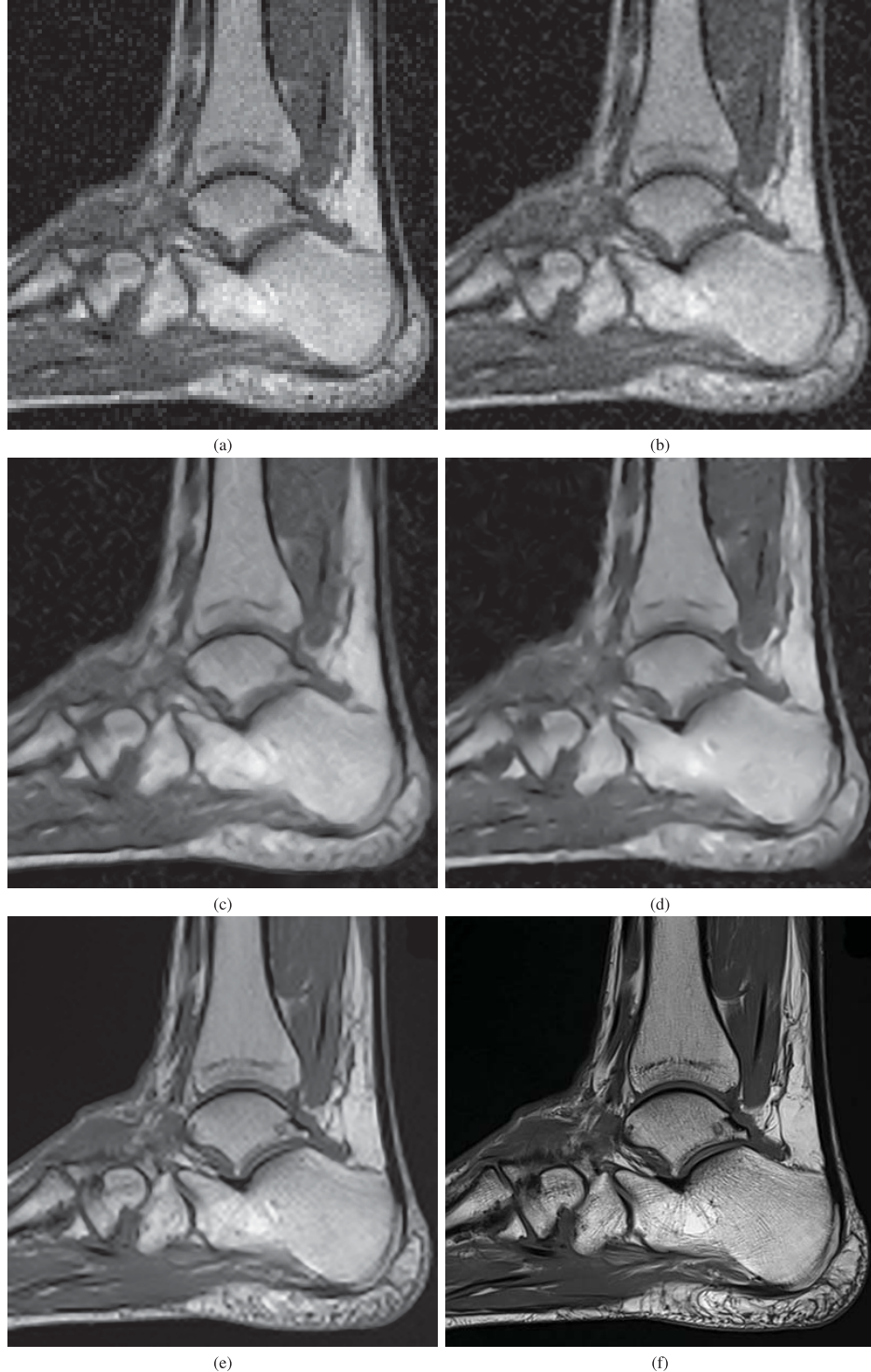


Fig. 3. Results on the MRI image of ankle [Fig. 1(d)] with magnification factor of 4. (a) LR image (size 100×100) corrupted by Gaussian noise with $\sigma = 10$ (shown with nearest neighbor interpolation). (b) Result of the bicubic interpolation (PSNR = 22.63 dB, SSIM = 0.56). (c) Result of the NE method [24] with the number of neighbors $K = 10$ (PSNR = 23.34 dB, SSIM = 0.58). (d) Result of the ScSR method [30] with the regularization parameter $\lambda = 0.8$, (PSNR = 23.87 dB, SSIM = 0.62). (e) Result of the proposed SRSW method (PSNR = **25.40** dB, SSIM = **0.75**). (f) Original test image.

bicubic interpolation and the NE-based method, and slightly better compared with the ScSR method. As it can be seen, in all the cases of noise ($\sigma = 5, 10, 20$), both PSNR and SSIM of the SRSW method are significantly higher than those of the other methods.

To further illustrate the effectiveness of the proposed method, the $4\times$ magnification results of the MRI image of ankle with noise level $\sigma = 10$, the CT image of thorax with noise level $\sigma = 10$ and the MRI image of knee with noise level $\sigma = 20$ are shown in Figs. 3, 4, and 8, respectively. In Fig. 4

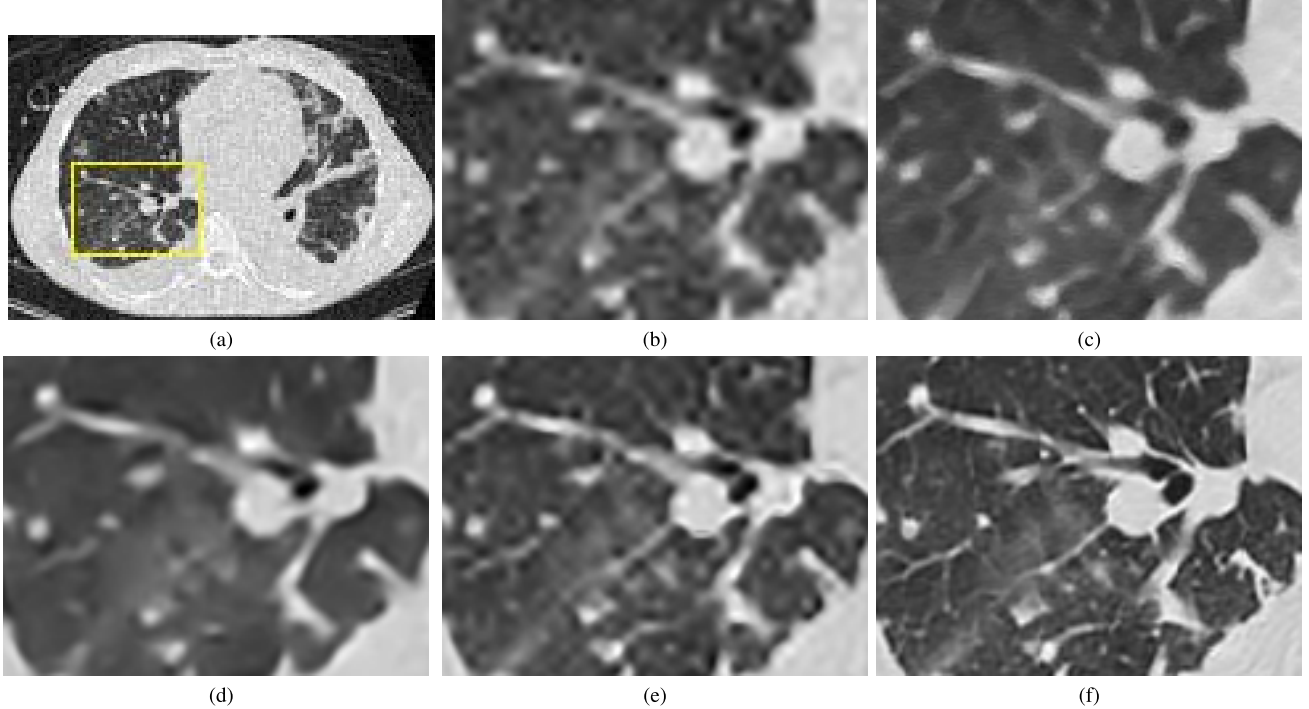


Fig. 4. The super-resolution results of a Desired Region Of Interest (DROI) of the CT image of thorax with magnification of 4 and noise level $\sigma = 10$. (a) LR image (size 135×90) in which the yellow rectangle illustrates a desired region of interest. (b)–(e) The DROI up-scaled by the Bicubic interpolation, the NE method [24] ($K = 7$), the ScSR method [30] ($\lambda = 0.8$), and the proposed SRSW method, respectively. (f) The DROI in the original test image.

we only show the SR results of a Desired Region Of Interest (DROI) of the LR image of thorax (the yellow rectangle in Fig. 4(a)). As expected, the result of Bicubic are blurred and noisy, as we can see in Figs. 3(b), 4(b), and Fig. 8(b). For noise level $\sigma = 10$, as shown in Figs. 3 and 4, the NE method and the ScSR method give good results with noises well suppressed, but many small details are removed. As it can be seen in Fig. 3(e), the proposed SRSW method gives the best results where noise is effectively reduced while well preserving many small details and contrast, compared to the original HR test image. This can be observed more clearly in Fig. 4(e).

For heavier noise level, Fig. 8 shows the experimental results on the MRI image of knee with a noise level $\sigma = 20$. The result of the NE method is very noisy and affected by noise-caused artefacts visible in homogeneous region, while many details and structures are modified or no longer discernable. The ScSR method [30] performs better denoising at the expense of over-smoothing small details and structures. The results of both the NE and ScSR methods can be explained by the fact that they use the feature vectors based on the gradient information of the LR patches. Because the LR patches are corrupted by noise, using gradient information is not thus confident. Therefore, the NE and ScSR methods generate unwanted artifacts [see Fig. 8(c) and 8(d)]. The result of the proposed SRSW method in Fig. 8(e), shows that noise is reduced while small details and structures are well preserved. Once again, the visual evaluation indicates excellent performance of the proposed method. All these

results demonstrate the ability and efficiency of our SRSW method in performing SR and denoising simultaneously. The results in case of images corrupted by different noise levels show that our proposed method outperforms the NE [24] and the ScSR [30] as well as the Bicubic.

C. Empirical Study on Parameters

In this subsection, we investigate the effects of some parameters on the performance of the proposed algorithm, namely the parameter γ in (28) and the regularization parameter λ in (31). Here, we take the Knee image [Fig. 1(e)] for example to study how the parameters influence the reconstructed results.

1) Effects of Regularization Parameter: To evaluate the effects of λ , we present the experiment of SR with magnification factor $s = 2$, for four noise levels $\sigma = 0, 5, 10$ and 20. Fig. 5 shows the behaviour of PSNR and SSIM versus several values of λ in $[0.000001 \ 0.00001 \ 0.0001 \ 0.0005 \ 0.001 \ 0.005 \ 0.01 \ 0.05 \ 0.1]$.

As observed, the PSNR and SSIM curves increase with λ in some first steps (around from 10^{-6} to 10^{-4}), and then noticeably reduce when λ increases from 0.01 to 0.1. The proposed method can achieve better performance when the regularization parameter is in the range between 0.0001 to 0.01. Especially, when $\lambda = 0.001$, all the PSNR and SSIM curves reach their peak values, except for the SSIM curve with $\sigma = 20$. Consequently, we use $\lambda = 0.001$ for all the experiments in our paper.

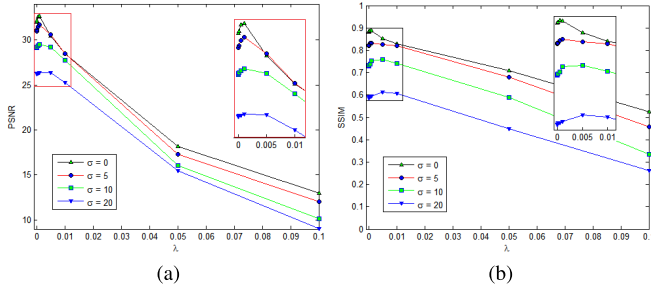


Fig. 5. PSNR and SSIM curves describing the effect of the regularization parameter λ on the SR performance. (a) PSNR. (b) SSIM.

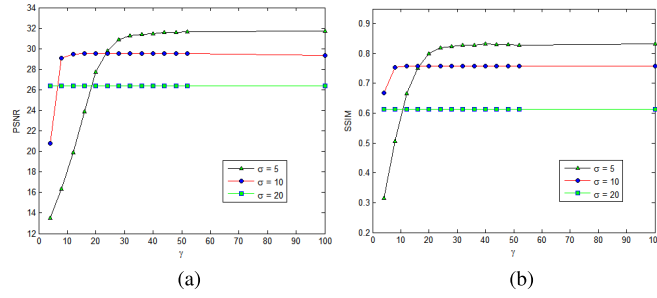


Fig. 6. Objective image quality measures with respect to different values of the parameter γ . PSNR and SSIM curves as the functions of parameter γ . (a) PSNR. (b) SSIM.

2) *Effects of Parameter γ* : The parameter γ in (28) affects the threshold ρ_i in (27), and thus the penalty coefficient w_{ik} in (21). Therefore, an important issue is how to determine a proper range of γ . For this purpose, we perform SR with magnification factor $s = 2$ on the Knee image with noise levels $\sigma = 5, 10$ and 20 . The impact of γ on the performance of the method is evaluated using PSNR and SSIM metrics for different values of γ , $\gamma \in [4 : 4 : 52] \cup \{100\}$ (here, $[4:4:52]$ means that γ takes the values from 4 to 52 with step 4). The experimental results are shown in Fig. 6.

From Fig. 6, we can see that for small noise ($\sigma = 5$), the PSNR and SSIM values increase smoothly within the range of γ from 4 to 40, and then they achieve the maximum value and stability for $\gamma \geq 44$. Similarly, for $\sigma = 10$, the PSNR and SSIM curves increase but in the smaller range [4:8], and attain stability for $\gamma \geq 8$. For higher noise level ($\sigma = 20$), the shape of the curves is almost horizontal. Therefore, the proper range of γ depends on the noise level. However, as it can be seen, we can choose $\gamma \geq 44$ to obtain the performance of the proposed SR method for all noise levels. That is why in our experiments, the parameter γ is set to 44.

D. Computational Complexity Analysis

As outlined in Algorithm 2, major cost of the proposed algorithm is in the implementation of Step 2, for N iterations. For each iteration, the computational complexity of Step 2(a) for computing the dissimilarity criteria $d(\mathbf{y}_i^l, \mathbf{u}_k^l)$ is $O(Mm)$. In Step 2(b), determining the subset \mathcal{I}_i consists in finding the K nearest \mathbf{u}_j^l in \mathbf{P}_l such that $d(\mathbf{y}_i^l, \mathbf{u}_j^l)$ are the first K smallest values, which yields $O(M \log M)$ complexity. Step 2(c) has $O(K)$ complexity. In Step 2(d) which includes Algorithm 1,

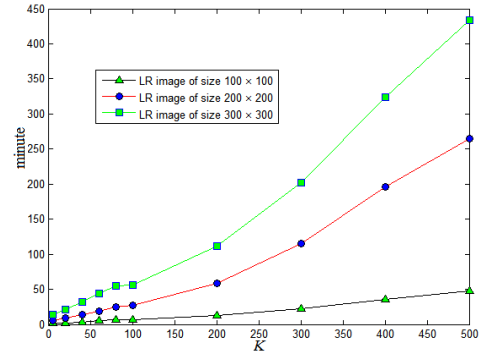


Fig. 7. The increasing of computational time via the increasing of K .

its complexity is $O(T(K^4m + 2Km + 2K + m))$ for obtaining the representation vector α^i . To generate the HR patch $\hat{\mathbf{x}}_i^h$ and the denoised LR patch $\hat{\mathbf{y}}_i^l$, Step 2(e) has a complexity of $O(K(m+n))$. As a result, the computational complexity of Step(2) is $O(NT(K^4m + 2Km + 2K + m) + NM \log M + NK(m+n))$. As the computational complexity of Algorithm 2 mainly depends on Step 2, this result is also the computational complexity of this algorithm.

Note that the computational complexity of the proposed method highly depends on the parameter of good candidates K . In order to verify this relationship experimentally, we have performed simulations with magnification factor $s = 2$ on three images of sizes 100×100 , 200×200 and 300×300 for several values of K ranging from 5 to 500. We used a database comprising 3850 LR and HR patch pairs. Simulation was performed on a laptop with an Intel Core i5 2.40GHz and 4GB RAM. Fig. 7 shows the overall computational time for various size of LR images and values of K . As expected, these curves show that for high value of K , the computational time increases polynomially. For small value of K , the curves describe a logarithmic behavior with slow variation, mainly due to the term $(NM \log M)$ which becomes dominant.

In order to compare the computational speed of the proposed method with the ScSR method [30] and the NE method [24], we have tested the three methods with magnification factor $s = 2$ on the Knee image of size 200×200 [Fig. 1(e)], using the same standard image of size 400×400 [Fig. 2(e)] to construct the example databases. All tests have been done using Matlab R2008a on a Lenovo ThinkPad T410 laptop with an Intel Core i5 2.40GHz and 4GB RAM. For the three methods, values of parameters are chosen to obtain good results. For the ScSR, it takes about 9 hours 20 minutes for training a dictionary of size 1000 elements from a database of 100000 examples. With the trained dictionary, the time for SR phase is about 3.5 minutes. For the NE method, with the number of nearest neighbors set to 7, the overall time for the NE method is about 37 minutes. For our method, with the database of size 3850 patch pairs and the parameter K set to 100, the overall computational time is about 27 minutes including the SR phase of 5 minutes. The computational time required in SR phase of the proposed method is slower than that of the ScSR method. This is also due to a high value of K and the fact that our implementation has not been optimized yet. However, the training phase of the proposed

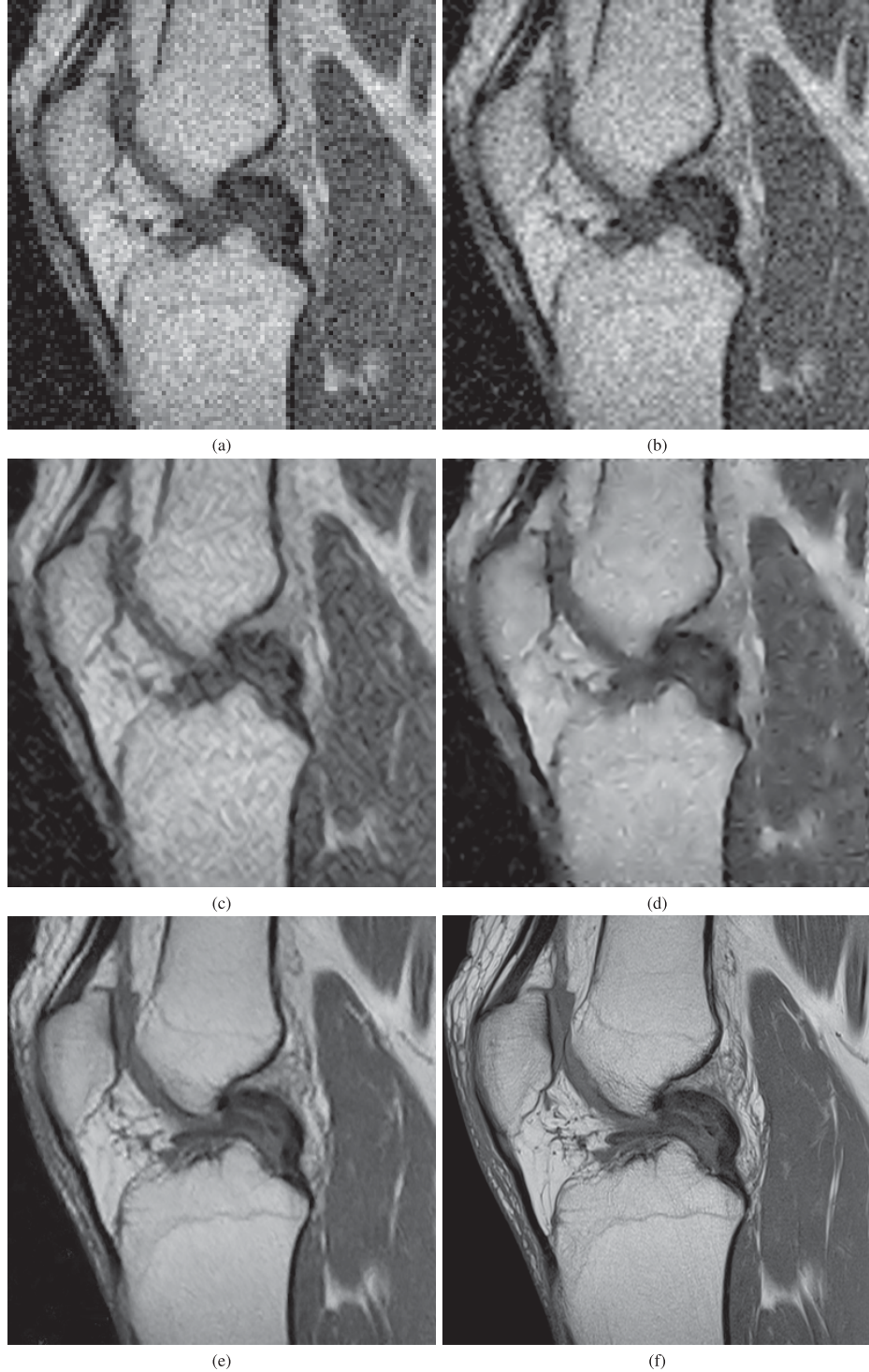


Fig. 8. Results on the MRI image of knee [Fig. 1(e)] with magnification factor of 4. (a) LR image (size 100×100) corrupted by Gaussian noise with $\sigma = 20$ (shown with nearest neighbor interpolation). (b) Result of Bicubic interpolation (PSNR = 22.16 dB, SSIM = 0.42). (c) Result of the NE method [24] with the number of neighbors $K = 4$ (PSNR = 23.16 dB, SSIM = 0.48). (d) Result of the ScSR method [30] with the regularization parameter $\lambda = 0.84$ (PSNR = 23.56 dB, SSIM = 0.52); (e) the proposed SRSW method (PSNR = **26.73** dB, SSIM = **0.68**); (f) Original HR test image.

method is not very time-consuming compared to the ScSR method. Comparing to the NE method, the proposed method is faster.

V. CONCLUSION

In this paper, we have proposed a very competitive example-based SR method capable of enhancing resolution while being

very robust to heavy noise. The method relies on the interesting idea that consists of using standard images (good quality, taken at the same organ as the given LR image, with the same medical imaging modality) to enhance the spatial resolution while denoising the given degraded and low-resolution image. Since medical images are specific, using this specificity for performing super-resolution allows more efficient solution than

a conventional SR method. These standard images are used as examples for the construction of the database of HR and LR patch pairs. Based on a sparse positive linear representation of the HR patches in the database, the problem is formulated as a sparse decomposition optimization problem with penalty function expressed in terms of dissimilarity between patches to enforce sparsity and the quality of the SR solution. In particular, a novel dissimilarity measure is proposed based on statistical properties of noise. The experimental results demonstrate the effectiveness of our method over several leading state-of-the-art SR methods. The proposed SRSW method is very useful for the case of noise-corrupted and low-resolution image. The results of the SRSW method for medical images are very promising, demonstrating the ability of the method for the potential improvement of diagnosis accuracy. In future works, we will study the construction of the training database of example patch pairs optimally from the given standard images.

REFERENCES

- [1] D. Bailey, P. Roach, E. Bailey, J. Hewlett, and R. Keijzers, "Development of a cost-effective modular SPECT/CT scanner," *Eur. J. Nucl. Med. Molecular Imag.*, vol. 34, no. 9, pp. 1415–1426, 2007.
- [2] G. Dougherty, *Digital Image Processing for Medical Applications*. Cambridge, U.K.: Cambridge Univ. Press, 2009.
- [3] D. Wallach *et al.*, "Super-resolution in 4D positron emission tomography," in *Proc. IEEE Nucl. Sci. Symp. Conf.*, Oct. 2008, pp. 4285–4287.
- [4] N. Ben-Eliezer, M. Irani, and L. Frydman, "Super-resolved spatially encoded single-scan 2D MRI," *Magn. Reson. Med.*, vol. 63, no. 6, pp. 1594–1600, 2010.
- [5] A. Gholipour, J. A. Estroff, and S. K. Warfield, "Robust super-resolution volume reconstruction from slice acquisitions: Application to fetal brain MRI," *IEEE Trans. Med. Imag.*, vol. 29, no. 10, pp. 1739–1758, Oct. 2010.
- [6] D. Kouame and M. Ploquin, "Super-resolution in medical imaging: An illustrative approach through ultrasound," in *Proc. IEEE Int. Symp. Biomed. Imag.*, Jul. 2009, pp. 249–252.
- [7] P. Akhtar and F. Azhar, "A single image interpolation scheme for enhanced super resolution in bio-medical imaging," in *Proc. 4th Int. CBBE*, Jun. 2010, pp. 1–5.
- [8] M. D. Robinson, S. J. Chiu, C. A. Toth, J. A. Izatt, J. Y. Lo, and S. Farsiu, "Super-resolution imaging," *Novel Applications of Super-Resolution in Medical Imaging*. Boca Raton, FL, USA: CRC Press, 2010, pp. 383–412.
- [9] H. S. Hou and H. C. Andrews, "Cubic splines for image interpolation and digital filtering," *IEEE Trans. Acoust., Speech Signal Process.*, vol. 26, no. 6, pp. 508–517, Dec. 1978.
- [10] R. G. Keys, "Cubic convolution interpolation for digital image processing," *IEEE Trans. Acoust., Speech, Signal Process.*, vol. 29, no. 6, pp. 1153–1160, Dec. 1981.
- [11] T. M. Lehmann, C. Gonner, and K. Spitzer, "Survey: Interpolation methods in medical image processing," *IEEE Trans. Med. Imag.*, vol. 18, no. 11, pp. 1049–1075, Nov. 1999.
- [12] S. C. Park, M. K. Park, and M. G. Kang, "Super-resolution image reconstruction: A technical overview," *IEEE Signal Process. Mag.*, vol. 20, no. 3, pp. 21–36, May 2003.
- [13] S. Farsiu, D. Robinson, M. Elad, and P. Milanfar, "Advances and challenges in super-resolution," *Int. J. Imag. Syst. Technol.*, vol. 14, no. 2, pp. 47–57, 2004.
- [14] J. Yang and T. Huang, "Super-resolution imaging," in *Image Super-Resolution: Historical Overview and Future Challenges*. Boca Raton, FL, USA: CRC Press, 2010.
- [15] T. Huang and R. Tsai, "Multi-frame image restoration and registration," *Adv. Comput. Vis. Image Process.*, vol. 1, no. 2, pp. 317–339, 1984.
- [16] M. Irani and S. Peleg, "Improving solution by image registration," *Comput. Vis., Graph. Image Process.*, vol. 53, no. 3, pp. 231–239, 1991.
- [17] M. Irani and S. Peleg, "Motion analysis for image enhancement: Resolution, occlusion and transparency," *J. Vis. Commun. Image Represent.*, vol. 4, no. 4, pp. 324–335, Dec. 1993.
- [18] S. Farsiu, M. D. Robinson, M. Elad, and P. Milanfar, "Fast and robust multi-frame super resolution," *IEEE Trans. Image Process.*, vol. 13, no. 10, pp. 1327–1344, Oct. 2004.
- [19] D. Glasner, S. Bagon, and M. Irani, "Super-resolution from a single image," in *Proc. ICCV*, 2009, pp. 349–356.
- [20] J. Sun, J. Sun, Z. Xu, and H. Shum, "Image super-resolution using gradient profile prior," in *Proc. IEEE CVPR*, Jun. 2008, pp. 1–8.
- [21] Y. W. Tai, S. Liu, M. S. Brown, and S. Lin, "Super resolution using edge prior and single image detail synthesis," in *Proc. IEEE CVPR*, Jun. 2010, pp. 2400–2407.
- [22] C. Y. Yang, J. B. Huang, and M. H. Yang, "Exploiting self-similarities for single frame super-resolution," in *Proc. ACCV*, 2010, pp. 497–510.
- [23] W. T. Freeman, T. R. Jones, and E. C. Pasztor, "Example-based super-resolution," *IEEE Comput. Graph. Appl.*, vol. 22, no. 2, pp. 56–65, Apr. 2002.
- [24] H. Chang, D. Yeung, and Y. Xiong, "Super-resolution through neighbor embedding," in *Proc. IEEE CVPR*, Jul. 2004, pp. 275–282.
- [25] T.-M. Chan, J. Zhang, J. Pu, and H. Huang, "Neighbor embedding based super-resolution algorithm through edge detection and feature selection," *Pattern Recognit. Lett.*, vol. 30, no. 5, pp. 494–502, Apr. 2009.
- [26] Y. Tang, P. Yan, Y. Yuan, and X. Li, "Single-image super-resolution via local learning," *Int. J. Mach. Learn. Cybern.*, vol. 2, no. 1, pp. 15–23, Mar. 2011.
- [27] X. Gao, K. Zhang, D. Tao, and X. Li, "Image super-resolution with sparse neighbor embedding," *IEEE Trans. Image Process.*, vol. 21, no. 7, pp. 3194–3205, Jul. 2012.
- [28] K. I. Kim and Y. Kwon, "Example-based learning for single-image super-resolution," in *Proc. DAGM*, 2008, pp. 456–465.
- [29] J. Yang, J. Wright, T. Huang, and Y. Ma, "Image super-resolution as sparse representation of raw image patches," in *Proc. IEEE CVPR*, Jun. 2008, pp. 1–8.
- [30] J. Yang, J. Wright, T. Huang, and Y. Ma, "Image super-resolution via sparse representation," *IEEE Trans. Image Process.*, vol. 19, no. 11, pp. 2861–2873, Nov. 2010.
- [31] R. Zeyde, M. Elad, and M. Protter, "On single image scale-up using sparse-representations," in *Proc. 7th Int. Curves Surf.*, 2010, pp. 711–730.
- [32] T. Goto, S. Suzuki, S. Hirano, M. Sakurai, and T. Q. Nguyen, "Fast and high quality learning-based super-resolution utilizing TV regularization method," in *Proc. IEEE ICIP*, Sep. 2011, pp. 1185–1188.
- [33] K. S. Ni and T. Q. Nguyen, "Image super-resolution using support vector regression," *IEEE Trans. Image Process.*, vol. 16, no. 6, pp. 1596–1610, Jun. 2007.
- [34] D. H. Trinh, M. Luong, J.-M. Rocchisani, C. D. Pham, H. D. Pham, and F. Dibos, "Image resolution enhancement by projection onto convex hull," in *Proc. 12th IEEE ISSPIT*, Ho Chi Minh City, Vietnam, Dec. 2012, to be published.
- [35] J. Yang, Z. Wang, Z. Lin, S. Cohen, and T. Huang, "Couple dictionary training for image super-resolution," *IEEE Trans. Image Process.*, vol. 21, no. 8, pp. 3467–3478, Aug. 2012.
- [36] J. Wang, S. Zhu, and Y. Gong, "Resolution enhancement based on learning the sparse association of image patches," *Pattern Recognit. Lett.*, vol. 31, no. 1, pp. 1–10, 2010.
- [37] D. H. Trinh, M. Luong, J.-M. Rocchisani, C. D. Pham, H. D. Pham, and F. Dibos, "An optimal weight model for single image super-resolution," in *Proc. Int. Conf. DICTA*, Fremantle, Australia, Dec. 2012, pp. 1–8.
- [38] W. Dong, L. Zhang, G. Shi, and X. Wu, "Image deblurring and super-resolution by adaptive sparse domain selection and adaptive regularization," *IEEE Trans. Image Process.*, vol. 20, no. 7, pp. 1838–1857, Jul. 2011.
- [39] M. Elad and M. Aharon, "Image denoising via sparse and redundant representations over learned dictionaries," *IEEE Trans. Image Process.*, vol. 15, no. 12, pp. 3736–3745, Dec. 2006.
- [40] D. H. Trinh, M. Luong, J.-M. Rocchisani, C. D. Pham, H. D. Pham, and F. Dibos, "An optimal weight method for CT image denoising," *J. Electron. Sci. Technol.*, vol. 10, no. 2, pp. 124–129, Jun. 2012.
- [41] D. D. Muresan and T. Parks, "Adaptive principal components and image denoising," in *Proc. IEEE ICIP*, Sep. 2003, pp. 101–104.
- [42] C. Liu, W. T. Freeman, R. Szeliski, and S. B. Kang, "Noise estimation from a single image," in *Proc. IEEE CVPR*, vol. 1, Jun. 2006, pp. 901–908.
- [43] V. K. Potluru, S. M. Plis, M. Mørup, V. D. Calhoun, and T. Lane, "Efficient multiplicative updates for support vector machines," in *Proc. SDM*, 2009, pp. 1218–1229.

- [44] P. O. Hoyer, "Non-negative sparse coding," in *Proc. 12th IEEE Workshop NNSP*, Martigny, Switzerland, Sep. 2002, pp. 557–565.
- [45] S. Dai, M. Han, Y. Wu, and Y. Gong, "Bilateral back-projection for single image super resolution," in *Proc. IEEE Int. Conf. Multimedia Expo*, Jul. 2007, pp. 1039–1042.
- [46] Z. Wang, A. C. Bovik, H. R. Sheikh, and E. P. Simoncelli, "Image quality assessment: From error visibility to structural similarity," *IEEE Trans. Image Process.*, vol. 13, no. 4, pp. 600–612, Apr. 2004.



Dinh-Hoan Trinh received the B.S. degree in mathematics education from the Vietnam National University, Hanoi, the M.S. degree in mathematics from the Hanoi Institute of Mathematics, and the Ph.D. degree in signal and image processing from the Laboratoire Analyse, Géométrie et Applications, Université Paris 13, Sorbonne Paris Cité, France, in 2005, 2008, and 2013, respectively. He is currently a Researcher with the Center Informatics and Computing, Vietnam Academy of Science and Technology. His research interests include image restoration, superresolution, segmentation, sparse coding, machine learning, optimization, and medical imaging.



Marie Luong received the Engineer Diploma degree from the Ecole Nationale Supérieure d'Electricité et de Mécanique de Nancy, France, and the Ph.D. degree in Automatic, Diagnosis, Signal processing from the L'Institut National Polytechnique de Lorraine (Lorraine University), France, in 1991 and 1996, respectively. She is currently an Associate Professor with the Université Paris 13, Sorbonne Paris Cité, France. Her research interests include image restoration, superresolution, segmentation, watermarking, and medical imaging.



Françoise Dibos is currently a Full Professor in applied mathematics with the Université Paris 13, Sorbonne Paris Cité, France. Her research interests include mathematical modelization for image processing, projective analysis and video analysis in real time, and medical imaging.



Jean-Marie Rocchisani received the Doctorate degree in medicine and the Ph.D. degree in applied mathematics in 1980 and 1985, respectively. He is currently a Medical Imaging Specialist with the Avicenne University Hospital, Bobigny, France, and an Assistant Professor of Biophysics with Université Paris 13. His research interest is medical image processing.



Canh-Duong Pham received the M.S. degree from the State University of Byelorussia, USSR, Moscow, Russia, and the Ph.D. degree in mathematics from the Computer Center of the Academy of Science, USSR, in 1973 and 1983, respectively. From 1973 to 1979, he was with the Institute of Mathematics, Hanoi, Vietnam. From 1980 to 1984, he was a Researcher and Post-Graduate Study with the Computer Center of the Academy of Sciences in Moscow. From 1984 to 2009, he was a Researcher with the Institute of Mathematics, Hanoi. Since 2009, he has been a Specialist with the Center for Informatics and Computing, Vietnam Academy of Science and Technology. His research interests include control theory, mathematical programming, and signal processing.



Truong Q. Nguyen is currently a Professor with the Electrical and Computer Engineering Department, University of California, San Diego. His current research interests include 3-D video processing and communications, and their efficient implementation. He is the co-author (with Prof. Gilbert Strang) of a popular textbook *Wavelets and Filter Banks* (Wellesley-Cambridge Press, 1997), and the author of several MATLAB-based toolboxes on image compression, electrocardiogram compression, and filter bank design. He has over 400 publications.

Prof. Nguyen received the IEEE Transaction in Signal Processing Paper Award (Image and Multidimensional Processing area) for the paper he co-wrote with Prof. P. P. Vaidyanathan on linear-phase perfect-reconstruction filter banks in 1992. He received the NSF CAREER Award in 1995 and is currently the Series Editor (Digital Signal Processing) for Academic Press. He served as an Associate Editor for the IEEE TRANSACTION ON SIGNAL PROCESSING from 1994 to 1996, the *Signal Processing Letters* from 2001 to 2003, the IEEE TRANSACTION ON CIRCUITS AND SYSTEMS from 1996 to 1997 and from 2001 to 2004, and the IEEE TRANSACTION ON IMAGE PROCESSING from 2004 to 2005.